NANO LETTERS

pubs.acs.org/NanoLett Letter

Chiral Guided Mode Resonance with Independently Controllable Quality Factor and Circular Dichroism

Zhancheng Li, Shiwang Yu, Guangzhou Geng, Jiaqi Cheng, Wenwei Liu, Yuebian Zhang, Junjie Li, Hua Cheng,* and Shuqi Chen*

Cite This: *Nano Lett.* 2025, 25, 2519−2527 Read Online

ACCESS | Metrics & More | Article Recommendations | Supporting Information

ABSTRACT: Chiroptical resonances with high quality factors (Q factors) have recently garnered extensive attention due to their broad applications in lasing and optical sensing. However, the independent manipulation of the Q factor and circular dichroism (CD) of chiroptical resonances has rarely been proposed. Here, we demonstrate that the Q factor and CD of guided mode resonance (GMR) can be independently manipulated by simply varying two structural parameters in a diatomic dielectric metasurface grating, offering a new paradigm for chiroptical resonance manipulation. We reveal that the independent manipulation of the Q factor and CD of the GMR is attributed to the modulation of the collective interference of guided mode fields excited by the two orthogonal linearly polarized normal incidence. GMRs with a Q factor of 183 and CD of ±0.62 have been experimentally validated, which is comparable to state-of-the-art chiral quasi-BICs. These findings provide a powerful platform for the realization of high-Q chiroptical resonances.

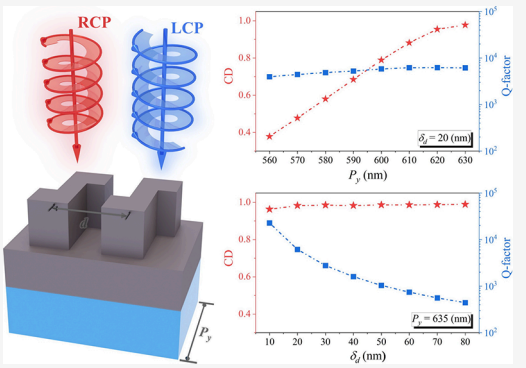

KEYWORDS: *Chiral metasurface, Guided mode resonance, Chiroptical response, High quality factor, Circular dichroism*

Recent developments in artificial micro- and nanostructures have demonstrated their remarkable ability to achieve high quality factor (Q factor) optical resonances, enabling effective light confinement and enhancing light−matter interactions.[1−4] Specifically, in metasurfaces composed of artificial nanostructures at subwavelength scales, this capability is significantly enhanced through the utilization of bound states in the continuum (BICs),[5−7] guided mode resonances (GMRs),[8,9] higher-order Mie resonances,[10] and surface lattice resonances (SLRs).[11,12] These resonances, characterized by narrow resonant peaks or low radiation losses, have been proposed as powerful platforms for the realization of low-threshold nanoscale lasers,[13−15] enhanced nonlinear and high-harmonic generation,[16,17] polarization manipulation in momentum space,[18,19] unidirectional radiation,[20] optical trapping,[21] and ultrasensitive hyperspectral imaging and biodetection.[22,23]

Nowadays, chiral high-Q resonances in metasurfaces have drawn significant attention from the research community due to their unprecedented capabilities for spin-selective light manipulation, chiral light emission, and optical biosensing.[24−27] Intrinsic chiral quasi-BICs with ultrahigh Q factors and near-unity circular dichroism (CD) have been numerically proposed by leveraging the collective interference of far-field radiation from two nanoresonators or by modulating the eigenpolarizations of quasi-BICs supported by nanoresonators while breaking all structural mirror symmetries.[28,29] However, the experimental implementation of such chiral quasi-BICs at optical wavebands requires advanced nanofabrication techniques and demands high precision in fabrication, hindering their broader application.[30,31] More importantly, the independent control of the Q factor and CD of the chiral resonance, which is essential for tailoring chiral resonances arbitrarily, has been rarely reported. Recent advances in achieving independent manipulation of the Q factor and CD of chiral quasi-BICs have focused on adjusting the relative height and rotation angle between two nanoresonators.[31,32] However, for designing metasurface arrays with tailored chiroptical properties for applications such as chiral sensing and detection, modulating the height of the nanostructures is not an optimal approach due to fabrication precision and cost considerations. A theoretical study has shown that a diatomic metasurface grating can support GMRs with high Q factors and near-unity CD, offering a promising alternative for achieving chiral high-Q resonances.[33] This metasurface grating consists of periodic nanostructures arranged on a planar waveguide slab, making their fabrication compatible with established nanofabrication

Received: December 2, 2024
Revised: January 28, 2025
Accepted: January 28, 2025
Published: January 31, 2025

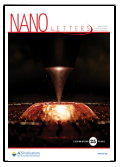

https://doi.org/10.1021/acs.nanolett.4c06157
Nano Lett. 2025, 25, 2519−2527

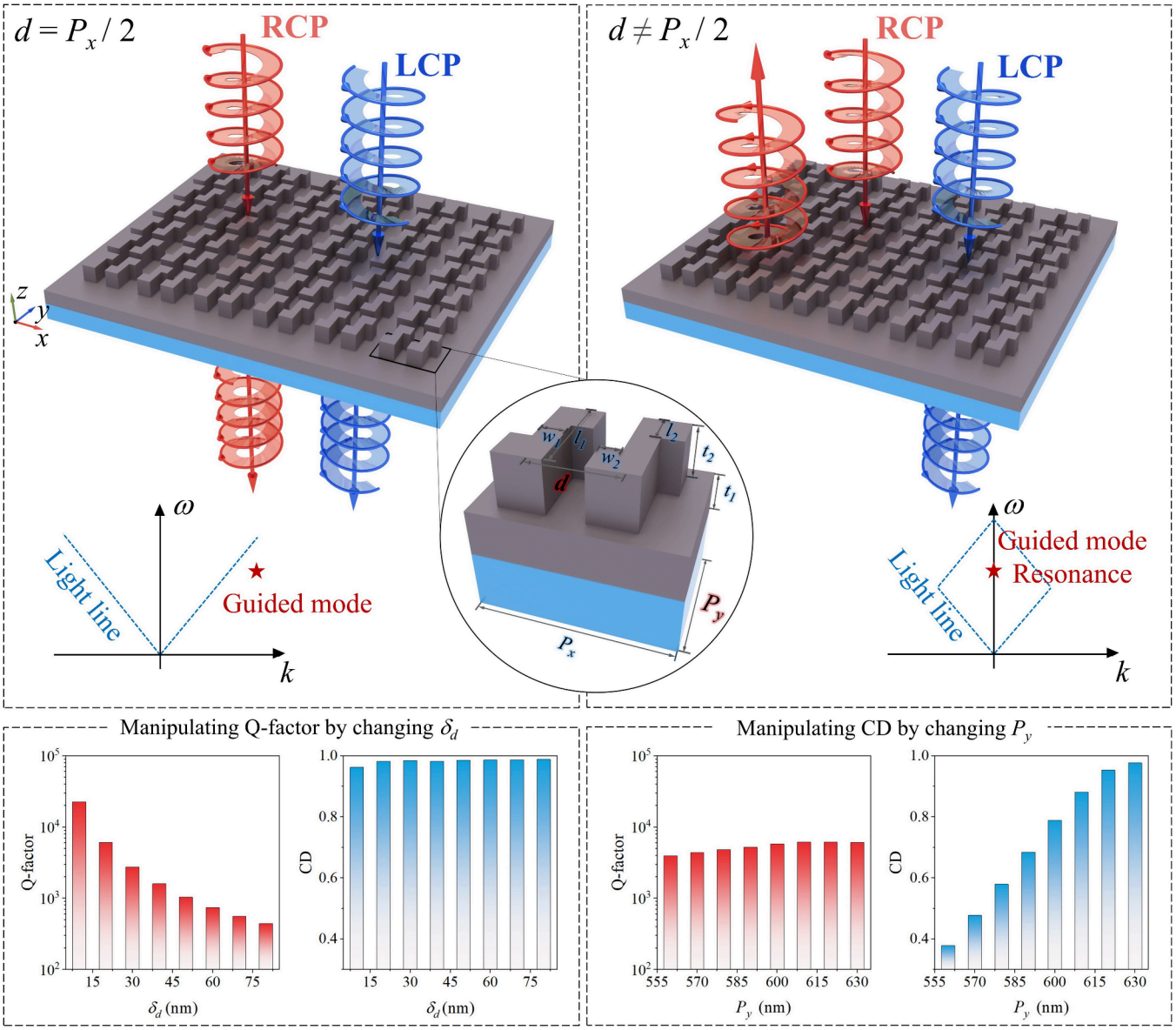

Figure 1. Schematic illustrating the chiral GMR induced by Brillouin zone folding and collective interference of guided mode fields. Upper plane: Schematic illustration of chiral GMR realization through Brillouin zone folding by doubling the structural period along the *x*-axis. Lower left (right) plane: the variation of the Q factor (defined as $Q = \omega_0/\Delta\omega$) and CD (defined as the transmission difference between left circularly polarized (LCP) and right circularly polarized (RCP) waves ($\Delta T = T_{LCP} - T_{RCP}$)) of GMR at the resonant wavelength with the changing of the asymmetric parameter δ_d (period P_y) while P_y = 635 nm (δ_d = 20 nm). Here, we assume an $e^{i\omega t}$ time dependence of electromagnetic fields, and LCP and RCP waves are defined such that the electric field at a fixed position *z* rotates in a clockwise or counterclockwise direction, respectively, when viewed from the direction toward which the wave is approaching.

techniques.[21,34] However, precise nanoscale control over the relative positioning of the two nanostructures within each unit cell of the metasurface grating is required, which poses significant fabrication challenges. On the other hand, the relative positioning of the two nanostructures affects both the Q factor and CD of the GMR, hindering their independent manipulation. The experimental realization of high-Q chiral GMRs has not yet been achieved, and the independent manipulation of the Q factor and CD of GMRs remains a significant challenge.

Here, we propose an efficient strategy for the realization of a GMR with independently controllable Q factor and CD using diatomic metasurface gratings with intrinsic geometric chirality. Specifically, the unit cells of these metasurface gratings, made from amorphous silicon (*α*-Si), consist of a planar slab and two Z-shaped nanostructures. The GMR with a high Q factor and near-unity CD can be achieved by adjusting the distance between the two Z-shaped nanostructures. Notably, we demonstrate that the Q factor of the GMR can be continuously tuned by varying this distance, while the CD and resonant wavelength remain constant. Additionally, the CD of the GMR can be continuously adjusted by modulating the period of the unit cell, while the Q factor and resonant wavelength remain nearly unchanged. We theoretically and numerically reveal that the GMR originates from Brillouin zone folding, and its CD results from the spin-selective collective interference of the guided mode fields excited by the transverse electric (TE) and transverse magnetic (TM)

https://doi.org/10.1021/acs.nanolett.4c06157
Nano Lett. 2025, 25, 2519−2527

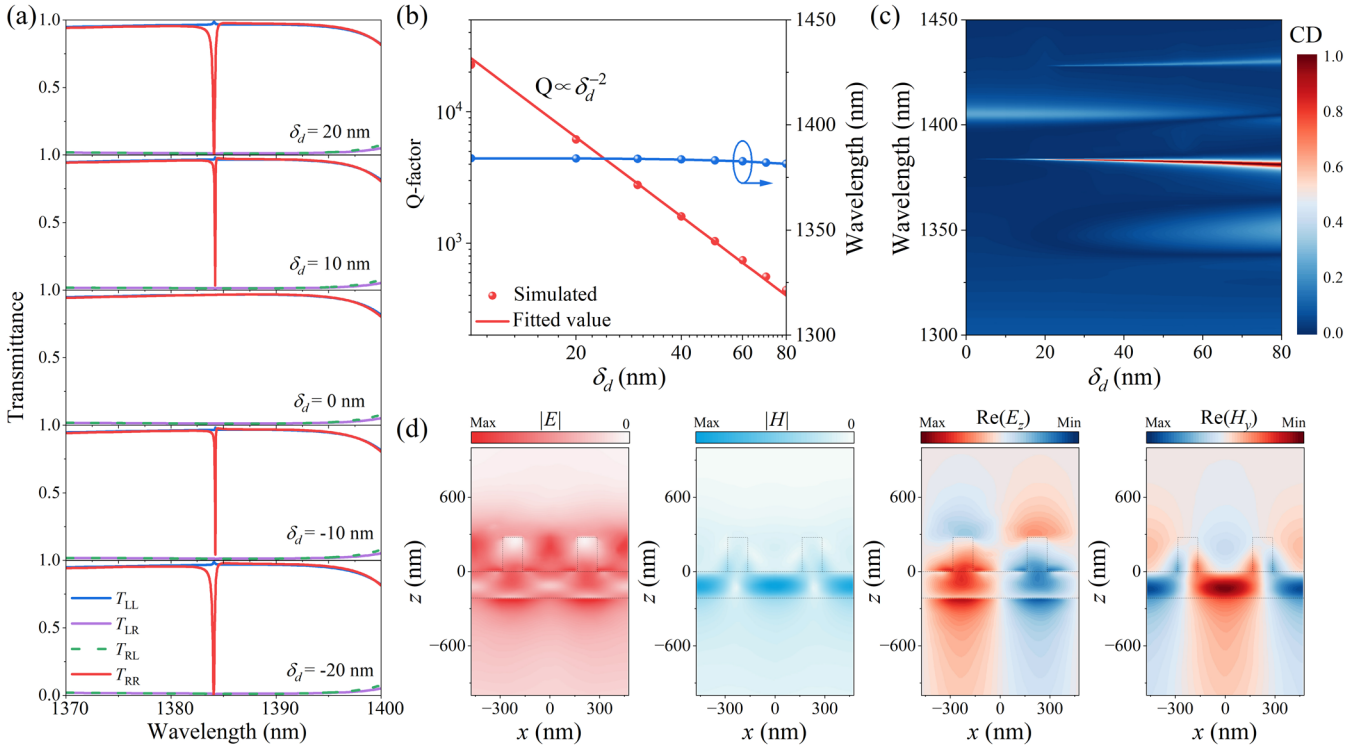

Figure 2. Characterization of the chiral GMR in the designed metasurface. (a) Simulated transmission spectra for different values of δ_d. (b) Variation of the Q factor and resonant wavelength of the GMR with increasing δ_d. (c) Variation of the CD spectrum with increasing δ_d. (d) Simulated distributions of the magnitude of the electric field and magnetic field, as well as the real part of the z-component of the electric field and the y-component of the magnetic field, on the x−z plane (y = 0 nm, the middle section of the unit cell) at the resonant wavelength under RCP illumination.

components of circularly polarized illumination. We further validate experimentally and realize chiral GMRs with a Q factor of 183 and CD of ±0.62. Our approach establishes a simple one-to-one correspondence between the Q factor and CD of a GMR and two structural parameters, providing a powerful platform for designing high-Q resonances with tailored chiroptical properties.

The structural configuration of the designed diatomic metasurface grating is shown in Figure 1. The unit cells of the designed metasurface grating consist of two Z-shaped nanostructures and a planar thin slab, both made of α-Si, on a SiO_2 substrate. The structural parameters are P_x = 950 nm, P_y = 635 nm, l_1 = 500 nm, l_2 = 150 nm, w_1 = 120 nm, w_2 = 180 nm, t_1 = 215 nm, and t_2 = 275 nm. The refractive indices of α-Si and SiO_2 were taken as 3.49 and 1.44 in the numerical analysis, respectively. When the distance d between the two adjacent Z-shaped nanostructures is not equal to $P_x/2$, the structural period along the x axis doubles. As a result, the guided mode at the edge of the first Brillouin zone appears at the Γ point due to Brillouin zone folding, becoming a GMR whose Q factor can be continuously tuned by changing the asymmetric parameter $\delta_d = P_x/2 - d$. Furthermore, the Z-shaped nanostructures can effectively couple both TM and TE light (corresponding to x-polarized and y-polarized light under normal incidence, respectively) into the GMR. The intensity ratio between excited guided mode fields for TE and TM waves can be continuously modulated by varying the structural period P_y, enabling controllable spin-selective collective interference of the guided mode fields and allowing for tunable CD. Consequently, the CD and Q factor of the GMR can be independently manipulated by changing P_y and δ_d, as validated by the simulated results in Figure 1.

We first analyze the characteristics of the chiroptical resonance observed in the designed metasurface grating. The simulated transmission spectra for different polarization components T_{ij} under LCP and RCP normal illumination are shown in Figure 2(a). The subscripts "i" and "j" in T_{ij} represent the polarization states of the transmitted and incident light, respectively. A chiroptical resonance with a small full width at half-maximum (FWHM) and near-unity CD can be observed in the transmission spectra when $\delta_d \neq 0$. Note that we defined CD based on the transmission difference $\Delta T = T_{LCP} - T_{RCP}$ instead of the normalized transmission difference $(T_{LCP} - T_{RCP})/(T_{LCP} + T_{RCP})$ used in some previous works, because the former is more suitable for characterizing maximum chirality.[30,31] This chiroptical resonance is an intrinsic chiroptical response, as the CD arises from the difference between T_{LL} and T_{RR}, while T_{LR} and T_{RL} are both equal to zero. It can be found that the FWHM of the chiroptical resonance increases with the increase of $|\delta_d|$, indicating an increasing Q factor. Meanwhile, the resonant wavelength remains unchanged as the δ_d increases. To further elucidate their relationship, we simulated the variation in the Q factor and resonant wavelength as the asymmetric parameter δ_d changes. As shown in Figure 2(b), the Q factor and the asymmetric parameter δ_d follow an inverse quadratic law: $Q = Q_0/\delta_d^2$, where Q_0 is a constant determined by the resonant mode and its interaction with the incident light. In contrast, the resonant wavelength remains unaffected by changes in δ_d, which is highly beneficial for applications in nanolasing and enhancing nonlinear harmonic generation.[35,36] Notably, the

https://doi.org/10.1021/acs.nanolett.4c06157
Nano Lett. 2025, 25, 2519−2527

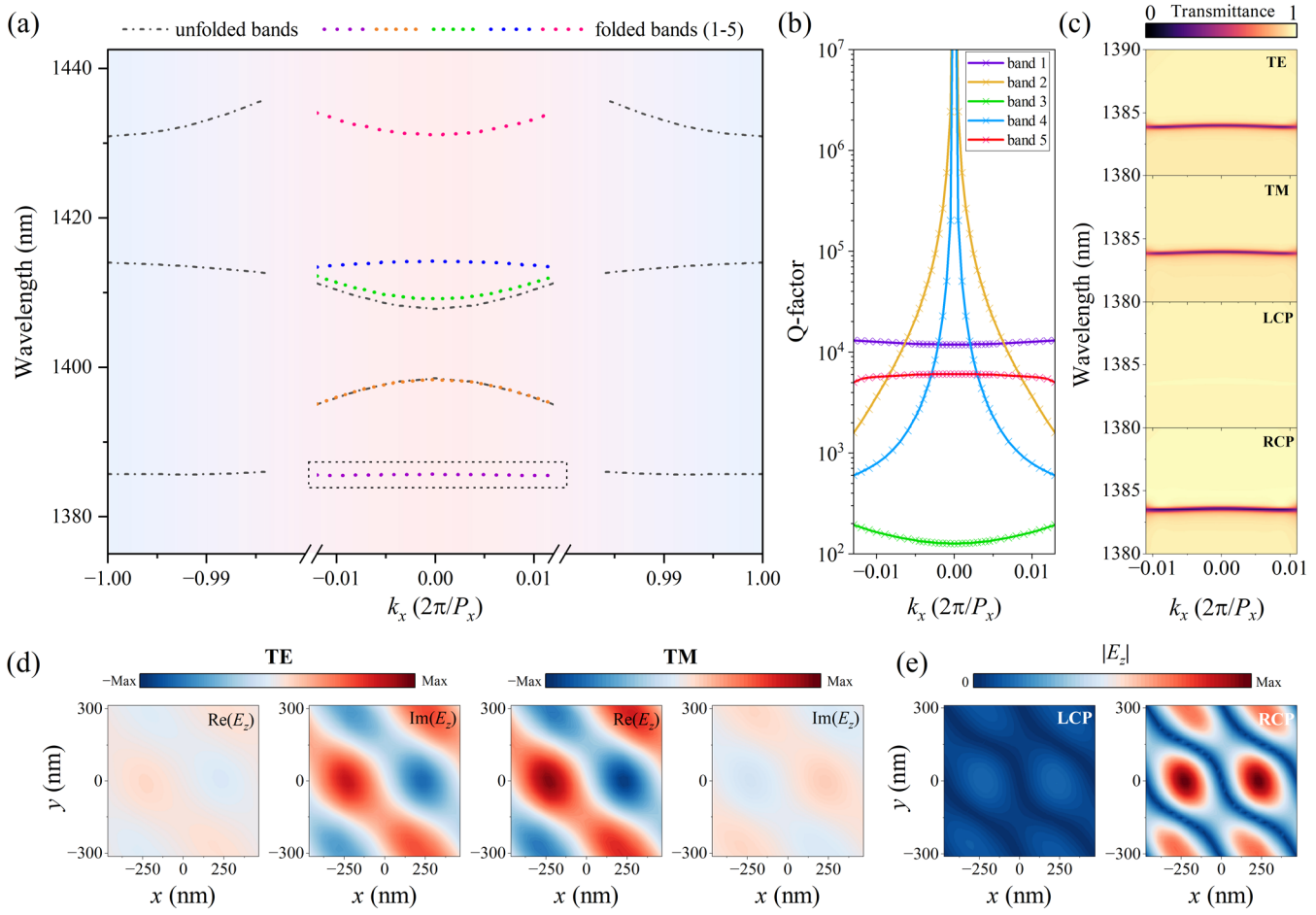

Figure 3. Physical mechanism behind the generation of chiral GMR. (a) Band structure of the designed metasurface grating for δ_d = 0 nm and δ_d = 20 nm, represented by gray dotted lines (unfolded bands) and colorful scatter lines (folded bands), respectively. (b) Simulated Q factors of folded bands. (c) Simulated transmittance-momentum spectra of the designed metasurface grating with δ_d = 20 nm under illumination with different polarization states. (d) Simulated distributions of the real and imaginary parts of the z-component of the electric field on the middle cross section of the α-Si slab at the resonant wavelength under TE (y-polarized) and TM (x-polarized) normal incidence. (e) Simulated distributions of the magnitude of the z-component of the electric field on the middle cross section of the α-Si slab at the resonant wavelength under LCP and RCP normal incidence.

value of CD at the resonant wavelength also remains unchanged as δ_d increases, as validated by the results in Figure 2(c). These findings demonstrate that the Q factor of the chiroptical resonance of interest can be effectively manipulated by varying δ_d, while the resonant wavelength and CD value remain constant. The mode of the chiroptical resonance is further verified by simulating the distributions of the electric and magnetic field magnitudes along the longitudinal section of one unit cell. As shown in Figure 2(d), enhanced electric and magnetic fields are observed near the metasurface grating. Specifically, the z-component of the electric field (E_z) and the x- and y-components of the magnetic field (H_x and H_y) are significantly enhanced; the enhanced magnetic field is localized within the planar thin slab, indicating the excitation of a TM-like GMR, confirming that the chiroptical resonance of interest is a GMR.[37−39]

To uncover the underlying physics behind the realization of chiral GMR, we calculated the band structure of the designed metasurface grating for δ_d = 0 nm and δ_d = 20 nm, as shown in Figure 3(a). When δ_d = 0 nm, the distance between the two Z-shaped nanostructures in each unit cell equals $P_x/2$. Consequently, the period of the metasurface grating along the x-direction is $P_x/2$. When δ_d = 20 nm, the distance d between the two adjacent Z-shaped nanostructures in each unit cell is less than $P_x/2$, causing the structural period along the x-axis to double and become P_x. As a result, guided modes at the edge of the first Brillouin zone, which lie below the light line, appear at the Γ point due to the Brillouin zone folding. It can be observed that there are two resonance modes at the Γ point when δ_d = 0 nm and five resonance modes at the Γ point when δ_d = 20 nm, including three folded modes. For δ_d = 20 nm, we designate the five bands corresponding to the five resonance modes as folded bands 1 to 5. We further simulated the Q factors of these folded bands, as illustrated in Figure 3(b). The results indicate that bands 1 and 5 correspond to two folded GMRs, for which their Q factors remain nearly unchanged as the magnitude of the x-component of the wavevector (k_x) increases.[9] Bands 2 and 4 are symmetry-protected BICs, where the relationship between the Q factor and k_x follows an inverse quadratic law, $Q \propto k^{-2}$.[38] The resonance mode of band 3 is a leaky mode with a low Q factor. The mode of the folded band 1 is the chiral GMR of interest, while the modes of the other bands are also chiral modes with different values of CD, as shown in Figure S1 of the Supporting Information (SI). The results in Figures 3(a) and 3(b) confirm that the chiral GMR of interest originates from the Brillouin zone folding.

https://doi.org/10.1021/acs.nanolett.4c06157
Nano Lett. 2025, 25, 2519−2527

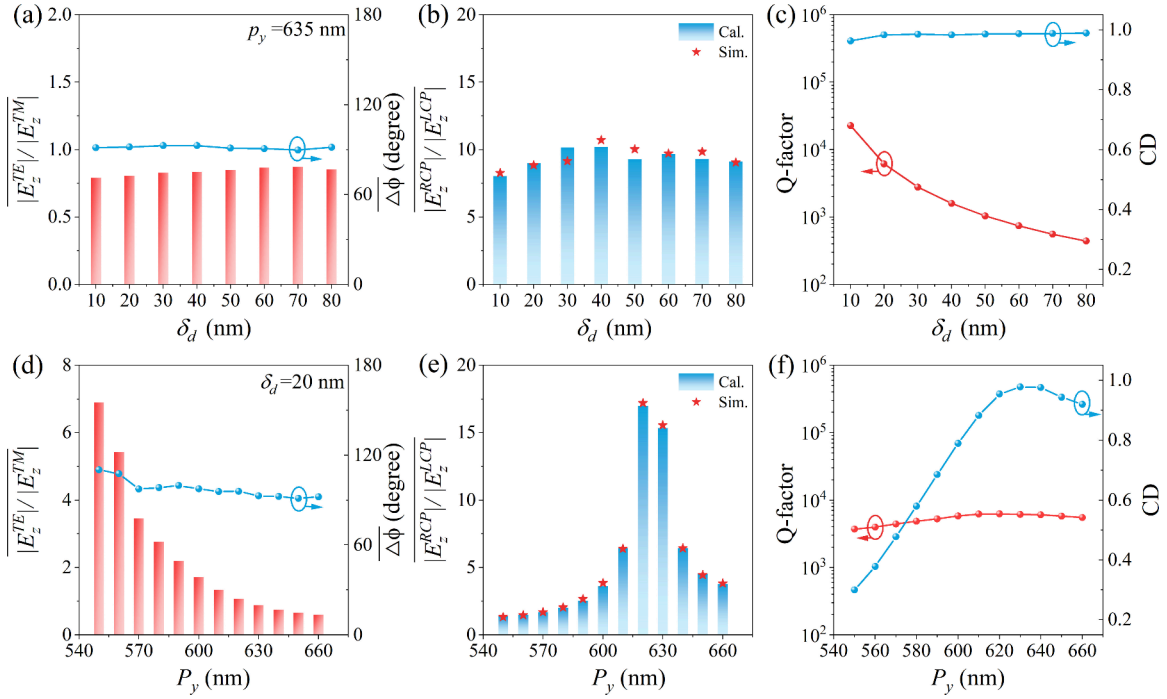

Figure 4. Independent manipulation of the CD and Q factor of the chiral GMR. Calculated mean values of the magnitude ratio and phase difference of the z-component of the electric field on the middle cross section of the α-Si slab at the resonant wavelength under TE and TM normal incidence for different values of (a) δ_d and (d) P_y. Calculated and simulated mean values of the magnitude ratio of the z-component of the electric field on the middle cross section of the α-Si slab at the resonant wavelength under LCP and RCP normal incidence for different values of (b) δ_d and (e) P_y. The variation of the Q factor of GMR and CD at the resonant wavelength with increasing (c) δ_d and (f) P_y.

Moreover, band 1 exhibits a flat region for $|k_x|$ lower than 0.0115. Chiral flat bands have recently garnered significant attention from the research community. A chiral flat band with a quasi-BIC mode has been reported in a metasurface grating with a similar structural configuration to our proposed design, where the realization of the chiral flat band is attributed to the modulation of the coupling between modes within the nanostructures and the planar slab by changing the structural symmetry and adjusting the structural parameters.[34] In contrast, the chiral flat band we obtained here is related to a GMR caused by Brillouin zone folding and the origin of chirality is different, as discussed below.

To further elucidate why the GMR is a chiral resonance, we first simulated the transmittance-momentum spectra of the designed metasurface grating with δ_d = 20 nm under illumination with different polarization states. As shown in Figure 3(c), transmission dips are observed under TE, TM, and RCP illumination, indicating the excitation of the GMR, while it cannot be excited by the LCP wave. We attribute this spin-selective excitation of the GMR to the collective interference of the guided mode fields excited by the TE and TM components of circularly polarized light. To validate our concept, we simulated the distributions of the real and imaginary parts of the z-component of the electric field (E_z) at the middle cross-section of the planar thin slab at the resonant wavelength under TE and TM normal incidence. The results in Figure 3(d) demonstrate that the same GMR can be excited by both TE and TM normal incidence, with the strength of the excited guided mode fields being similar, while a phase delay close to $\pi/2$ between them is observed. Since LCP and RCP waves can be decomposed into TM and TE components with a phase delay of $\pm\pi/2$, the phase difference between the guided mode fields excited by the TM and TE components of LCP and RCP waves is π and 0, respectively, resulting in destructive and constructive interference. Consequently, the coupling strength (quantitatively described by $|E_z|$) of the GMR under LCP and RCP illumination is eliminated and enhanced, respectively, as validated by the simulated results in Figure 3(e). Specifically, the $|E_z|$ of the excited guided mode fields at the middle cross section of the planar thin slab under LCP and RCP illumination can be obtained based on the equations $|E_z^{TM}(1 + E_z^{TE}/E_z^{TM})|$, where E_z^{TE} and E_z^{TM} represent E_z of the guided mode fields excited by the TE and TM components of the LCP and RCP waves. The TE and TM components of the LCP and RCP waves, illuminated along the −z direction (as shown in Figure 1), exhibit phase differences ($\Delta\varphi = \varphi_{TE} - \varphi_{TM}$) of $\pi/2$ and $-\pi/2$, respectively, while the guided mode fields excited by the TE and TM waves have a phase difference of $\pi/2$. Consequently, the phase differences between E_z^{TE} and E_z^{TM} are π and 0 for LCP and RCP waves, respectively. Since the amplitudes of $E_z^{TE}$and E_z^{TM} are nearly equal, $|E_z|$ under LCP and RCP illumination can be expressed as 0 and $2|E_z^{TM}|$, respectively. $|E_z| = 0$ indicates the elimination of GMR excitation (weak coupling strength) and a near-unity transmittance, while $|E_z| = 2|E_z^{TM}|$ signifies enhanced GMR excitation (strong coupling strength) and a high reflectance, consistent with the results shown in Figures 2(a) and 3(e). We further calculated the distributions of $|E_z|$ under LCP and RCP illumination based on the simulated results in Figure 3(d). The calculated results (see Figure S2 in SI) align well with the simulated data in Figure 3(e), further validating the collective interference effect.

To demonstrate the effectiveness of our theory for realizing high-Q chiral GMR, we analyze the collective interference of guided mode fields in our design for various values of δ_d. As illustrated in Figure 4(a), the magnitude ratio and phase

https://doi.org/10.1021/acs.nanolett.4c06157
Nano Lett. 2025, 25, 2519−2527

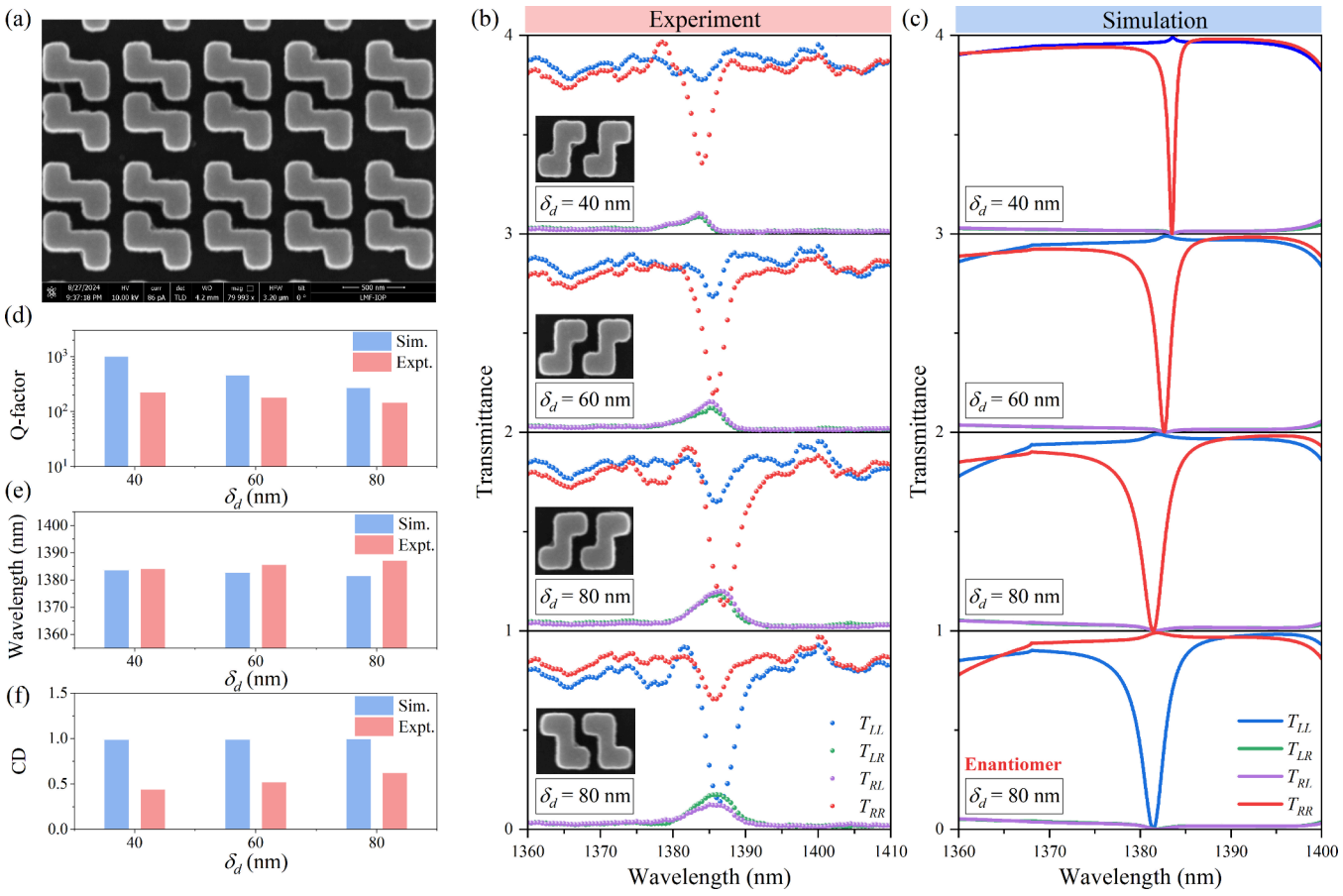

Figure 5. Experimental verification of the high-Q chiral GMR in the designed metasurface. (a) SEM image of the fabricated sample with δ_d = 80 nm. (b) Measured and (c) simulated transmission spectra for different values of δ_d and for the enantiomer of the proposed design with δ_d = 80 nm. Measured and simulated (d) Q factor and (e) resonant wavelength of the GMRs and (f) CD at the resonant wavelengths for different values of δ_d.

difference between E_z^{TE} and E_z^{TM} remain nearly constant, approximately 0.75 and $\pi/2$, respectively. According to the collective interference model discussed earlier, this stable magnitude ratio and phase difference indicate a consistent ratio between $|E_z|$ under LCP and RCP illumination, as validated by the results in Figure 4(b). Notably, although the magnitudes of E_z^{TE} and E_z^{TM} gradually decrease with increasing δ_d (see Figure S3 in SI), the coupling between the TE and TM waves with the GMR remains sufficiently strong to yield a transmittance close to zero under RCP illumination. Consequently, the CD remains unchanged with an increasing δ_d. Additionally, the Q factor and the asymmetric parameter δ_d follow an inverse quadratic law, $Q = Q_0/\delta_d^2$, due to the nature of the GMR. Therefore, the Q factor of the chiral GMR can be adjusted by varying δ_d while keeping the CD near unity and the resonant wavelength unchanged. Meanwhile, we find that the magnitude ratio between $E_z^{TE}$and E_z^{TM} can be manipulated by changing structural parameter P_y, while keeping their phase difference close to $\pi/2$, thus providing an effective means for controlling the CD of the chiral GMR. As shown in Figure 4(d), the magnitude ratio between E_z^{TE} and E_z^{TM} gradually decreases with increasing P_y, while their phase difference remains close to $\pi/2$. Consequently, the ratio of $|E_z|$ under LCP and RCP illumination first increases and then decreases with increasing P_y, as validated by the simulated and calculated results in Figure 4(e). This ratio reflects the coupling strength between the GMR and the LCP and RCP waves with variations leading to changes in CD, as shown in Figure 4(f). On the other hand, the Q factor remains unchanged, while the resonant wavelength changes slightly with increasing P_y (see Figure S4 in SI). Thus, the CD of the chiral GMR can be adjusted by varying P_y while keeping the Q factor constant. The slight change in the resonant wavelength can be further modulated by adjusting other structural parameters (see Figures S5 and S6 in SI). Overall, the Q factor and CD of the chiral GMR can be independently manipulated by changing δ_d and P_y, respectively, as further validated by the results in Section 5 of the SI. This provides an effective approach for implementing high-Q chiral resonances.

We further validate the high-Q chiral GMRs in the proposed metasurface gratings by fabricating three samples with δ_d = 40, 60, and 80 nm, while keeping P_y = 635 nm, along with an enantiomer of the design with δ_d = 80 nm. The details regarding the fabrication process of samples and the measurement of transmission spectra can be found in Section 6 of the SI. The scanning electron microscope (SEM) image of the fabricated metasurface grating with δ_d = 80 nm is shown in Figure 5(a). The edges of the Z-shaped nanostructures appear somewhat rough, and the structural parameters of the fabricated samples are slightly larger than those designed. The measured transmission spectra of the fabricated samples, presented in Figure 5(b), confirm the existence of a high-Q chiral resonance, with the Q factor decreasing as δ_d increases. Notably, the proposed design with δ_d = 80 nm and its enantiomer exhibit opposite CD, indicating that the sign of the CD can be modulated by using the proposed designs and their

https://doi.org/10.1021/acs.nanolett.4c06157
Nano Lett. 2025, 25, 2519−2527

enantiomers. The results also confirm that the structural symmetry of the Z-shaped nanostructures plays a crucial role in manipulating the CD of the chiral GMR. Variations in structural symmetry alter the collective interference effect and consequently modify the CD of the GMR (Figure S7 in SI). The measured results align reasonably well with the simulated data shown in Figure 5(c). Although T_{LR} and T_{RL} are small but not zero at the resonant wavelength, indicating the existence of a polarization conversion effect, discrepancies between the simulated and measured spectra can be attributed mainly to fabrication imperfections, particularly the slight difference in the refractive index of α-Si used in the numerical simulation and that of the fabricated samples. Figures 5(d) and 5(e) compare the measured and simulated Q factors, resonant wavelengths, and CD at the resonant wavelength. Both simulated and measured Q factors decrease with increasing δ_d, but measured Q factors are lower than the simulated ones. The resonant wavelengths remain constant in both cases, though the measured wavelengths exhibit a slight red-shift compared to simulated values. The simulated CD at the resonant wavelength remains constant with increasing δ_d, while the measured CD increases, a phenomenon previously noted in other high-Q resonators due to lower coupling strengths between resonators and light in experiments.[40−42] The measured results could be further improved by addressing the fabrication imperfections. Overall, a chiroptical resonance with a Q factor of 183 and CD of ±0.62 has been experimentally validated based on the proposed design with δ_d = 80 nm, which is comparable to state-of-the-art chiral quasi-BICs,[31] demonstrating the efficacy of our design for high-Q chiral resonance implementation.

In summary, we demonstrated that chiral GMRs with controllable Q factor and CD can be achieved using a diatomic dielectric metasurface grating. We showed that the GMRs in the designed metasurface grating arise from Brillouin zone folding, while their CD results from spin-selective collective interference of the guided mode fields excited by the TE and TM components of circularly polarized illumination. Consequently, the Q factor and CD of the GMRs can be independently and continuously manipulated by adjusting two structural parameters, δ_d and P_y, respectively. Our design strategy can be summarized in two steps: first, obtaining a GMR with a controllable Q factor through Brillouin zone folding in diatomic nanostructures; and second, modulating the CD of the GMR by controlling the intensity ratio and phase difference of the guided mode fields excited by TE and TM polarized incidence. Overall, the advantages of our approach can be summarized as two key points: First, our strategy provides an efficient method for realizing high-Q chiral GMRs. The Q factor and CD can be effectively and independently tuned. Second, the designed metasurface grating significantly reduces structural complexity compared to state-of-the-art approaches, lowering fabrication requirements and enabling compatibility with widely used nanofabrication techniques. This approach offers a powerful platform for designing high-Q chiral resonances with potential applications in chiral lasing and nonlinear harmonic wave manipulation.

■ ASSOCIATED CONTENT

Supporting Information

The Supporting Information is available free of charge at https://pubs.acs.org/doi/10.1021/acs.nanolett.4c06157.

Analysis on the CD of the excited resonances in the wavelength region of interest; calculated guided mode fields under LCP and RCP normal illumination based on the collective interference model; variation in coupling strength between the GMR and both the TE and TM normal incidence, as well as the resonant wavelength, as a function of δ_d and P_y; variation of CD spectrum with the changing of structural parameters; validation of the independent manipulation of the Q factor and CD of the chiral GMR by changing δ_d and P_y; details of sample fabrication and transmission spectra measurement (PDF)

■ AUTHOR INFORMATION

Corresponding Authors

Hua Cheng − *The Key Laboratory of Weak Light Nonlinear Photonics, Ministry of Education, School of Physics and TEDA Institute of Applied Physics, Nankai University, Tianjin 300071, China*; Email: hcheng@nankai.edu.cn

Shuqi Chen − *The Key Laboratory of Weak Light Nonlinear Photonics, Ministry of Education, School of Physics and TEDA Institute of Applied Physics, Nankai University, Tianjin 300071, China; School of Materials Science and Engineering, Smart Sensing Interdisciplinary Science Center, Nankai University, Tianjin 300350, China; The Collaborative Innovation Center of Extreme Optics, Shanxi University, Taiyuan, Shanxi 030006, China;* orcid.org/0000-0002-7898-4148; Email: schen@nankai.edu.cn

Authors

Zhancheng Li − *The Key Laboratory of Weak Light Nonlinear Photonics, Ministry of Education, School of Physics and TEDA Institute of Applied Physics, Nankai University, Tianjin 300071, China*

Shiwang Yu − *The Key Laboratory of Weak Light Nonlinear Photonics, Ministry of Education, School of Physics and TEDA Institute of Applied Physics, Nankai University, Tianjin 300071, China*

Guangzhou Geng − *Beijing National Laboratory for Condensed Matter Physics, Institute of Physics, Chinese Academy of Sciences, Beijing 100190, China*

Jiaqi Cheng − *The Key Laboratory of Weak Light Nonlinear Photonics, Ministry of Education, School of Physics and TEDA Institute of Applied Physics, Nankai University, Tianjin 300071, China*

Wenwei Liu − *The Key Laboratory of Weak Light Nonlinear Photonics, Ministry of Education, School of Physics and TEDA Institute of Applied Physics, Nankai University, Tianjin 300071, China*

Yuebian Zhang − *The Key Laboratory of Weak Light Nonlinear Photonics, Ministry of Education, School of Physics and TEDA Institute of Applied Physics, Nankai University, Tianjin 300071, China*

Junjie Li − *Beijing National Laboratory for Condensed Matter Physics, Institute of Physics, Chinese Academy of Sciences, Beijing 100190, China;* orcid.org/0000-0002-1508-9891

Complete contact information is available at: https://pubs.acs.org/10.1021/acs.nanolett.4c06157

Notes

The authors declare no competing financial interest.

https://doi.org/10.1021/acs.nanolett.4c06157
Nano Lett. 2025, 25, 2519−2527

■ ACKNOWLEDGMENTS

This work was supported by the National Key Research and Development Program of China (2021YFA1400601 and 2024YFA1409903), the National Natural Science Fund for Distinguished Young Scholar (11925403), and the National Natural Science Foundation of China (12122406, 12192253, 12274237, 12274239, and U22A20258).

■ REFERENCES

(1) Hsu, C. W.; Zhen, B.; Stone, A. D.; Joannopoulos, J. D.; Soljačić, M. Bound states in the continuum. *Nat. Rev. Mater.* **2016**, *1*, 16048.
(2) Oudich, M.; Kong, X.; Zhang, T.; Qiu, C.-W.; Jing, Y. Engineered moiré photonic and phononic superlattices. *Nat. Mater.* **2024**, *23*, 1169−1178.
(3) Wang, B.; Yu, P.; Wang, W.; Zhang, X.; Kuo, H. C.; Xu, H.; Wang, Z. M. High-Q plasmonic resonances: fundamentals and applications. *Adv. Opt. Mater.* **2021**, *9*, 2001520.
(4) Tian, J.; Li, Q.; Belov, P. A.; Sinha, R. K.; Qian, W.; Qiu, M. High-Q all-dielectric metasurface: super and suppressed optical absorption. *ACS Photonics* **2020**, *7*, 1436−1443.
(5) Jin, J.; Yin, X.; Ni, L.; Soljačić, M.; Zhen, B.; Peng, C. Topologically enabled ultrahigh-Q guided resonances robust to out-of-plane scattering. *Nature* **2019**, *574*, 501−504.
(6) Kang, M.; Zhang, S.; Xiao, M.; Xu, H. Merging bound states in the continuum at off-high symmetry points. *Phys. Rev. Lett.* **2021**, *126*, 117402.
(7) Yu, S.; Li, Z.; Chai, R.; Liu, W.; Zhou, W.; Cheng, H.; Chen, S. Merging bound states in the continuum in the geometrical parameter space. *Phys. Rev. B* **2024**, *109*, 115109.
(8) Huang, L.; Jin, R.; Zhou, C.; Li, G.; Xu, L.; Overvig, A.; Deng, F.; Chen, X.; Lu, W.; Alù, A.; Miroshnichenko, A. E. Ultrahigh-Q guided mode resonances in an All-dielectric metasurface. *Nat. Commun.* **2023**, *14*, 3433.
(9) Sun, K.; Wang, W.; Han, Z. High-Q resonances in periodic photonic structures. *Phys. Rev. B* **2024**, *109*, No. 085426.
(10) Hail, C. U.; Foley, M.; Sokhoyan, R.; Michaeli, L.; Atwater, H. A. High quality factor metasurfaces for two-dimensional wavefront manipulation. *Nat. Commun.* **2023**, *14*, 8476.
(11) Bin-Alam, M. S.; Reshef, O.; Mamchur, Y.; Alam, M. Z.; Carlow, G.; Upham, J.; Sullivan, B. T.; Ménard, J.-M.; Huttunen, M. J.; Boyd, R. W.; Dolgaleva, K. Ultra-high-Q resonances in plasmonic metasurfaces. *Nat. Commun.* **2021**, *12*, 974.
(12) Lim, T.-L.; Vaddi, Y.; Bin-Alam, M. S.; Cheng, L.; Alaee, R.; Upham, J.; Huttunen, M. J.; Dolgaleva, K.; Reshef, O.; Boyd, R. W. Fourier-engineered plasmonic lattice resonances. *ACS Nano* **2022**, *16*, 5696−5703.
(13) Wu, M.; Ding, L.; Sabatini, R. P.; Sagar, L. K.; Bappi, G.; Paniagua-Domínguez, R.; Sargent, E. H.; Kuznetsov, A. I. Bound state in the continuum in nanoantenna-coupled slab waveguide enables low-threshold quantum-dot lasing. *Nano Lett.* **2021**, *21*, 9754−9760.
(14) Huang, C.; Zhang, C.; Xiao, S.; Wang, Y.; Fan, Y.; Liu, Y.; Zhang, N.; Qu, G.; Ji, H.; Han, J.; Ge, L.; Kivshar, Y.; Song, Q. Ultrafast control of vortex microlasers. *Science* **2020**, *367*, 1018−1021.
(15) Chai, R.; Liu, W.; Li, Z.; Zhang, Y.; Wang, H.; Cheng, H.; Tian, J.; Chen, S. Spatial Information Lasing Enabled by Full-k-space Bound States in the Continuum. *Phys. Rev. Lett.* **2024**, *132*, 183801.
(16) Koshelev, K.; Kruk, S.; Melik-Gaykazyan, E.; Choi, J. H.; Bogdanov, A.; Park, H. G.; Kivshar, Y. Subwavelength dielectric resonators for nonlinear nanophotonics. *Science* **2020**, *367*, 288−292.
(17) Zograf, G.; Koshelev, K.; Zalogina, A.; Korolev, V.; Hollinger, R.; Choi, D.-Y.; Zuerch, M.; Spielmann, C.; Luther-Davies, B.; Kartashov, D.; Makarov, S. V.; Kruk, S. S.; Kivshar, Y. High-harmonic generation from resonant dielectric metasurfaces empowered by bound states in the continuum. *ACS Photonics* **2022**, *9*, 567−574.
(18) Liu, W.; Wang, B.; Zhang, Y.; Wang, J.; Zhao, M.; Guan, F.; Liu, X.; Shi, L.; Zi, J. Circularly polarized states spawning from bound states in the continuum. *Phys. Rev. Lett.* **2019**, *123*, 116104.
(19) Qin, H.; Su, Z.; Liu, M.; Zeng, Y.; Tang, M.-C.; Li, M.; Shi, Y.; Huang, W.; Qiu, C.-W.; Song, Q. Arbitrarily polarized bound states in the continuum with twisted photonic crystal slabs. *Light: Sci. & Appl.* **2023**, *12*, 66.
(20) Yin, X.; Jin, J.; Soljačić, M.; Peng, C.; Zhen, B. Observation of topologically enabled unidirectional guided resonances. *Nature* **2020**, *580*, 467−471.
(21) Le, N. D.; Bouteyre, P.; Kheir-Aldine, A.; Dubois, F.; Cueff, S.; Berguiga, L.; Letartre, X.; Viktorovitch, P.; Benyattou, T.; Nguyen, H. S. Super Bound States in the Continuum on a Photonic Flatband: Concept, Experimental Realization, and Optical Trapping Demonstration. *Phys. Rev. Lett.* **2024**, *132*, 173802.
(22) Tittl, A.; Leitis, A.; Liu, M.; Yesilkoy, F.; Choi, D.-Y.; Neshev, D. N.; Kivshar, Y. S.; Altug, H. Imaging-based molecular barcoding with pixelated dielectric metasurfaces. *Science* **2018**, *360*, 1105−1109.
(23) Yesilkoy, F.; Arvelo, E. R.; Jahani, Y.; Liu, M.; Tittl, A.; Cevher, V.; Kivshar, Y.; Altug, H. Ultrasensitive hyperspectral imaging and biodetection enabled by dielectric metasurfaces. *Nat. Photonics* **2019**, *13*, 390−396.
(24) Zhang, X.; Liu, Y.; Han, J.; Kivshar, Y.; Song, Q. Chiral emission from resonant metasurfaces. *Science* **2022**, *377*, 1215−1218.
(25) Shi, T.; Deng, Z.-L.; Geng, G.; Zeng, X.; Zeng, Y.; Hu, G.; Overvig, A.; Li, J.; Qiu, C.-W.; Alù, A.; Kivshar, Y. S.; Li, X. Planar chiral metasurfaces with maximal and tunable chiroptical response driven by bound states in the continuum. *Nat. Commun.* **2022**, *13*, 4111.
(26) Qi, X.; Wu, J.; Wu, F.; Zhao, S.; Wu, C.; Min, Y.; Ren, M.; Wang, Y.; Jiang, H.; Li, Y.; Guo, Z.; Yang, Y.; Zheng, W.; Chen, H.; Sun, Y. Observation of maximal intrinsic chirality empowered by dual quasi-bound states in the continuum in a planar metasurface. *Photon. Res.* **2024**, *12*, 244−252.
(27) Deng, Q. M.; Li, X.; Hu, M. X.; Li, F. J.; Li, X.; Deng, Z. L. Advances on broadband and resonant chiral metasurfaces. *npj Nanophotonics* **2024**, *1*, 20.
(28) Gorkunov, M. V.; Antonov, A. A.; Kivshar, Y. S. Metasurfaces with maximum chirality empowered by bound states in the continuum. *Phys. Rev. Lett.* **2020**, *125*, No. 093903.
(29) Overvig, A.; Yu, N.; Alù, A. Chiral quasi-bound states in the continuum. *Phys. Rev. Lett.* **2021**, *126*, No. 073001.
(30) Chen, Y.; Deng, H.; Sha, X.; Chen, W.; Wang, R.; Chen, Y.-H.; Wu, D.; Chu, J.; Kivshar, Y. S.; Xiao, S.; Qiu, C.-W. Observation of intrinsic chiral bound states in the continuum. *Nature* **2023**, *613*, 474−478.
(31) Kühner, L.; Wendisch, F. J.; Antonov, A. A.; Bürger, J.; Hüttenhofer, L.; Menezes, L. de S.; Maier, S. A.; Gorkunov, M. V.; Kivshar, Y.; Tittl, A. Unlocking the out-of-plane dimension for photonic bound states in the continuum to achieve maximum optical chirality. *Light: Sci. & Appl.* **2023**, *12*, 250.
(32) Tang, Y.; Liang, Y.; Yao, J.; Chen, M. K.; Lin, S.; Wang, Z.; Zhang, J.; Huang, X. G.; Yu, C.; Tsai, D. P. Chiral bound states in the continuum in plasmonic metasurfaces. *Laser Photonics Rev.* **2023**, *17*, 2200597.
(33) Zhang, D.; Liu, T.; Lei, L.; Deng, W.; Wang, T.; Liao, Q.; Liu, W.; Xiao, S.; Yu, T. Tailoring intrinsic chirality in a two-dimensional planar waveguide grating via quasibound states in the continuum. *Phys. Rev. B* **2024**, *109*, 205403.
(34) Choi, M.; Alù, A.; Majumdar, A. "Observation of Photonic Chiral Flatbands. arXiv preprint arXiv:2408.09328, 2024. DOI: 10.48550/arXiv.2408.09328.
(35) Yang, J.-H.; Huang, Z.-T.; Maksimov, D. N.; Pankin, P. S.; Timofeev, I. V.; Hong, K.-B.; Li, H.; Chen, J.-W.; Hsu, C.-Y.; Liu, Y.-Y.; Lu, T.-C.; Lin, T.-R.; Yang, C.-S.; Chen, K.-P. Low-threshold bound state in the continuum lasers in hybrid lattice resonance metasurfaces. *Laser Photonics Rev.* **2021**, *15*, 2100118.
(36) You, S.; Zhou, M.; Xu, L.; Chen, D.; Fan, M.; Huang, J.; Ma, W.; Luo, S.; Rahmani, M.; Zhou, C.; Miroshnichenko, A. E.; Huang, L. Quasi-bound states in the continuum with a stable resonance wavelength in dimer dielectric metasurfaces. *Nanophotonics* **2023**, *12*, 2051−2060.

https://doi.org/10.1021/acs.nanolett.4c06157
Nano Lett. 2025, 25, 2519−2527

(37) Overvig, A. C.; Shrestha, S.; Yu, N. Dimerized high contrast gratings. *Nanophotonics* **2018**, *7*, 1157−1168.
(38) Jeon, D.; Rho, J. Quasi-Trapped Guided Mode in a Metasurface Waveguide for Independent Control of Multiple Nonlocal Modes. *ACS Photonics* **2024**, *11*, 703−713.
(39) Joseph, S.; Sarkar, S.; Khan, S.; Joseph, J. Exploring the optical bound state in the continuum in a dielectric grating coupled plasmonic hybrid system. *Adv. Opt. Mater.* **2021**, *9*, 2001895.
(40) Wang, W.; Srivastava, Y. K.; Tan, T. C.; Wang, Z.; Singh, R. Brillouin zone folding driven bound states in the continuum. *Nat. Commun.* **2023**, *14*, 2811.
(41) Zhang, Y.; Wang, L.; He, H.; Duan, H.; Huang, J.; Gao, C.; You, S.; Huang, L.; Miroshnichenko, A. E.; Zhou, C. High-Q magnetic toroidal dipole resonance in all-dielectric metasurfaces. *APL Photonics* **2024**, *9*, No. 076106.
(42) Du, X.; Xiong, L.; Zhao, X.; Chen, S.; Shi, J.; Li, G. Dual-band bound states in the continuum based on hybridization of surface lattice resonances. *Nanophotonics* **2022**, *11*, 4843−4853.

https://doi.org/10.1021/acs.nanolett.4c06157
Nano Lett. 2025, 25, 2519−2527